Available online at www.sciencedirect.com
SCIENCE DIRECT®
ELSEVIER
Nuclear Instruments and Methods in Physics Research B 239 (2005) 440–450
NIM B
Beam Interactions with Materials & Atoms
www.elsevier.com/locate/nimb

A stationary plasma thruster for modification of polymer and ceramic surfaces

J.Y. Park, Y.S. Jung, Yu.A. Ermakov [1], W.K. Choi *

Thin Film Materials Research Center, Korea Institute of Science and Technology, Cheongryang, P.O. Box 131, Seoul 130-650, South Korea

Received 25 March 2005; received in revised form 10 May 2005
Available online 14 July 2005

Abstract

A stationary plasma thruster (SPT)-type source with high plasma density is introduced and its physical principle and structure are briefly summarized. As general characteristic performance of the gridless SPT plasma source, ion current density, its angular distributions and distribution of ions over energies for three working gases of Ar, N_2 and O_2 was examined and also compared with that of a conventional Kaufman-type grid ion source. In order to investigate the possible application of SPT for the surface modification, polymer and ceramic surfaces are irradiated by the low energy and high fluence ion beam generated from SPT. The wetting angle of polyimide is greatly reduced from 78° to 2–4° by the irradiation of reactive O_2^+ and N_2O^+ ions with an average energy of 180 eV. Furthermore when α-Al_2O_3 (0 0 0 1) is irradiated by N_2^+ ion of SPT source at various ion fluences, the formation of new Al—ON and Al—N chemical bonding are identified by X-ray photoelectron spectroscopy. From the results, it is revealed that the SPT can be used as an effective ion source for the enhancement of surface energy of polymer and for the formation of functional groups on ceramic surface.

PACS: 41.75.A

Keywords: Stationary plasma thruster; Surface modification; Low energy high fluence; Ceramic surface; Polymer surface

1. Introduction

Various particle sources used in the present technology can be mainly divided in to two classes [1]: gridded sources and gridless ones. Both the types have their own merits and demerits. For example, gridded sources, having their origin from

* Corresponding author.
E-mail address: wkchoi@kist.re.kr (W.K. Choi).
[1] Permanent address: D.V. Skobeltsyn Institute of Nuclear Physics of the Lomonosov, Moscow State University, Moscow, Russia.

0168-583X/$ - see front matter © 2005 Elsevier B.V. All rights reserved.
doi:10.1016/j.nimb.2005.05.042

Kaufman-type ion source, show good performance with ions of rather high energy (more than 1 kV), but they give small ion current density (ICD) at the level of tens of microamperes per square centimeter. This is a principal consequence of space-charge limitation concerned with electrostatic acceleration of ions in their scheme. On the other hand, gridless sources accelerate the matter in the form of plasma and do not create sufficient space charge at any step of accelerating process, and thus the space-charge limitation is absent. It is easy to generate soft and dense (nearly 100 eV of energy and tens of mA/cm^2 of current density) ion beams from gridless sources. The stationary plasma thruster (SPT) sources received much attention in the recent past. In literature, the thruster is reported as "plasma accelerator with closed electron drift and prolonged acceleration zone" [2,3]. The SPT was invented and developed to an advanced state by Morozov et al. at Kurchatov Institute, Russia (then USSR) during 1960s [4]. The SPT is a low thrust (up to 100 mN) electric space-propulsion engine with high specific impulse (up to 2000 s). It can be used for on-orbit maneuvering of satellites and for long space trips starting from near-Earth orbit. The thrusters were used for the first time in the space on board of a satellite during 1971 and till now, they were employed for more than 50 launches of satellites in Russia with SPT as maneuvering engine. The work on SPT was started in USA and France recently during 1990 [5].

In this study, the physical concept and principles of SPT are briefly introduced and a wide angle SPT source was characterized in terms of ion current density using Ar, O_2 and N_2 gases. A reactive ion beam of SPT with low energy of 150–200 eV and high fluence of 0.5–4.5 mA/cm^2 was irradiated to modify polymer and ceramic surfaces, and the change of surface energy and the formation of new functional groups induced by an ion irradiation are studied.

2. Main physical processes in the SPT

A schematic of SPT-type ion source is shown in Fig. 1. Main parts of the ion source are as follows: (1) a magnetic system consisted of iron magnetic line guide and several magnetic coils, which can be operated in series with a main discharge or independently; (2) an annular ceramic channel where main ionization and acceleration processes take place; (3) anode which is combined with a gas distributor in the initial designs but in the later ones they are separated [3]; and (4) a cathode which usually a heated hole cathode with LaB_6 pellet for emitter, but may be a simple filament or hole cathode with heating from main discharge or hole cathode with additional discharge. In this study we used the latter one. The magnetic system creates approximately radial magnetic field having maximum field near the source outlet and decreasing field towards the source inlet where an anode is situated. Usually, the maximum of a magnetic flux density B_m lies in a range 150–300 Gauss. The form of the magnetic force lines inside the ceramic channel defines (with an accuracy to the electron temperature) the equipotential surfaces of the electric field and the direction of the ion acceleration. They should be convex towards the anode for

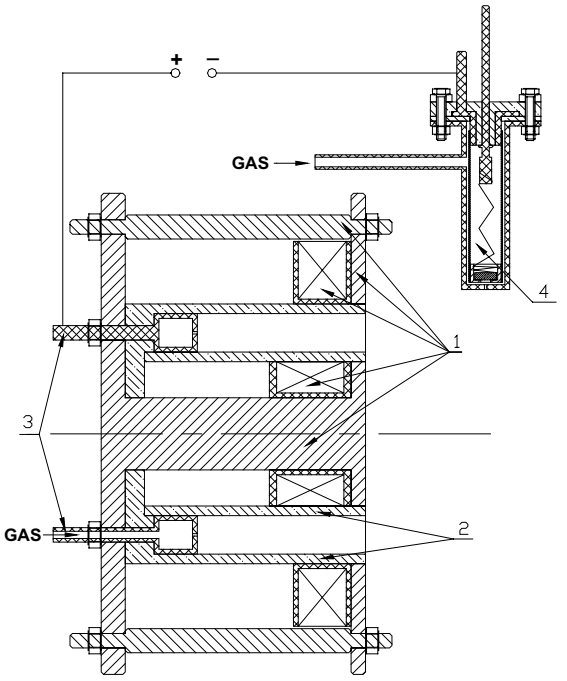

Fig. 1. Schematic diagram of the SPT-type plasma source: (1) a magnetic system, (2) an annular channel, (3) an anode with gas distributor and (4) a cathode.

creating convergent plasma beam. Magnetic field magnitude is chosen such that Larmor radius of electron (ρ_e) will be much less than the length of discharge gap L (distance between anode and cathode, about 3–4 cm in common SPT) and that of ion (ρ_i) much more than L ($\rho_e \ll L \ll \rho_i$). Usually, $L/\rho_e \approx 20$–30 and $\rho_i/L \approx 100$ in common SPT. These conditions imply the electrons are strongly affected by the magnetic field (magnetized) and not the ions. A role of the annular ceramic channel is dual. Firstly, the loss of electron's momentum due to its collisions with the channel walls contributes into electron transfer in the channel (in addition to the collisions with neutrals and ions in plasma volume). Secondly, the electron collisions with the channel walls impel the electrons to move circularly over cylindrical angle, creating Hall current. The Hall current is very important in SPT because the plasma acceleration may be described in terms of an Ampere–force interaction between the radial magnetic field and the angular Hall current:

$$\vec{f} = \vec{J} \times \vec{B}. \tag{1}$$

Main ionization processes take place in a zone near anode (gas distributor) where a plasma potential drop is approximately equal to 40–50 V (the main potential drop takes place in an acceleration zone near magnetic field maximum). A length of the zone of ionization is defined by $\lambda_i = v_0/(\langle \sigma_i |\vec{v}_r| \rangle_e n_e$, where v_0 is mean velocity of neutrals entering the channel, σ_i is an electron-impact ionization cross section, $|\vec{v}_r|$ is a modulus of relative velocity of the electron and the neutral, angle brackets $\langle \cdot \rangle_e$ means averaging over electron and neutral velocity distribution functions, and n_e is electron concentration. The λ_i is one of the main parameters of the SPT and its ratio to channel length ($\gamma = \lambda_i/L$) is the main scale parameter of the device. The effectiveness of the device is high if $\gamma \approx 1/3$–$1/4$ and it is low if $\gamma \geqslant 1$.

As mentioned above, most of the neutrals will get ionized in zone where voltage drop is 40–50 V from the net discharge voltage U_d. If recombination processes in the channel are negligible, as the volume recombination being three particles process in the plasma volume and at the walls it may become so with the proper design of magnetic field geometry, the energy distribution of ions variance at the SPT exit will be of the order of 50 V and this is experimentally reported elsewhere [2]. Mean ion energy in output flow can be estimated experimentally through the equation

$$\langle E_i \rangle \approx \left(\frac{2}{3} - \frac{3}{4}\right) e U_d, \tag{2}$$

where e is elementary charge and U_d is discharge voltage. The cathode compensates an output ion flow. Gas flow through the cathode creates plasma bridge between a cathode cavity and the output ion flow. The electron flow coming from the cathode divides into two parts: electrons going with ion beam and electrons going through channel towards anode. A current of the former is equal to ion current of the source, J_i and can be measured with Faraday cup situated to gather plasma beam and biased (-30 to -40 V) relative to the cathode. A current of the latter is equal to electron current, J_e. A net electron current from the cathode is equal to full discharge current, J_d:

$$J_d = J_i + J_e. \tag{3}$$

As an electric power going into the source $P = J_d U_d$ is a power loss, an efficiency of the source can be estimated with equation:

$$\eta = \frac{J_i}{J_d}. \tag{4}$$

The main parameter controlling the performance of the SPT as ion source, is ionization length [6]:

$$\lambda_i = \frac{1}{\langle \sigma_i v_e \rangle n_e} \sqrt{\frac{3RT_a}{M}}, \tag{5}$$

where σ_i is an ionization cross section, v_e is an electron velocity, n_e is an electron density, $\langle \cdot \rangle$ means averaging over an electron velocity distribution, T_a is neutral atom temperature, M is gas molar mass and R is molar gas constant. If λ_i is small compared with channel length, the effectiveness of ionization processes will be high and hence the better performance. Let us compare λ_i for different gases, for example, Ar and Xe. Since ionization constant $\langle \sigma_i v_e \rangle$ and molar mass for Xe are higher than those of Ar approximately by a factor of 2 and 3.28, respectively, the ratio of corresponding ionization rates is equal to

$$\frac{\lambda_i(\mathrm{Ar})}{\lambda_i(\mathrm{Xe})} \approx 2 \times \sqrt{3.28} \approx 3.6. \quad (6)$$

This relation indicates the reason why the source having good performance for Xe than Ar and other weakly ionizable gases. One of the ways to improve the performance of SPT with light noble gases is to enlarge plasma density n_e in the channel. However, this enlargement is limited often by pumping abilities of vacuum system available. One of the ways to avoid this limitation is to work with SPT in pulsed gas feeding operating mode [7].

3. Experiment

In this work we investigate SPT-type source designed and assembled in Moscow Institute of Radio-Engineering, Electronics and Automation (MIREA). The source was designed to obtain rather broad beam of Ar plasma. For this purpose, the annular insulator channel was made in the form of truncated cone and magnetic field was chosen so as to defocus the beam. The source was modified to extend the applicability of the device with other gases, except Ar. Initially, we used a hollow cathode with additional discharge (with LaB_6 powder emitter) and then igniter with high voltage (upto 15 kV in a peak, usually ignition voltage is the same as discharge voltage but ignition electrode situated near cathode). The low power SPT with weakly ionizable gases, always associated with an overheating of the device leading to low power efficiency of the source, as mentioned earlier. For example, argon usually exhibits 25–30% efficiency and the remaining 70% of the power is consumed for heating the source itself, where as Xe exhibits 50–65% efficiency. The problem of effective deflection of this power is yet to be solved.

The experiments are carried out with Ar, O_2 and N_2. Their masses, ionization coefficients and ionization potentials are rather close, hence it is expected that a similar performance of the source with all these gases. The overheating problem forces us not to increase the discharge current higher than 1.2 A. On the other hand, with the discharge current lower than 1 A, the source transits into rather unstable operating mode with strong fluctuations known as "circuit oscillations" [8]. So, we have only narrow band over discharge current to operate the source and can change operating modes by controlling over the discharge voltage and a gas flow rate together with keeping the current constant. With these conditions, we determine the dependence between gas flow rate and discharge voltage with constant discharge current (~1 A).

The ion current density distribution over an angle relative to the source axis is measured along the plane at distance 15 cm from the source outlet with a small Faraday cup having aperture of 7 mm^2. Discharge voltage (U_d) is varied for different gases to obtain maximum of the ICD along the source axis. Measurements are made with different gas flow rates within a range 4–8 sccm. Ion distributions over energy are measured with the same Faraday cup modified to repel the electrons.

The polyimide (PI) (Kapton-E, 38 μm) samples were irradiated with Ar^+, O_2^+ and N_2O^+ ions. The surface morphology of the irradiated samples was examined by an atomic force microscope (Nanoscope-IV, DI3100) and the change of surface energy is automatically calculated by measuring the wetting angle of deionized water and ethylene glycol using a Goniostar contact anglometer. Single crystal α-Al_2O_3(0 0 0 1) was also irradiated with N_2^+ ion at various ion fluences and the induced chemical bonding on the modified surface was identified by XPS (PHI-5700).

4. Results and discussion

4.1. Characterization of SPT

The dependence $U_d(q)$ of discharge voltage U_d on gas flow rate q with constant discharge current (1.1 A) for different gases is shown in Fig. 2. Note that the curve for Ar exhibits some signs of saturation, which show that the ionization processes in the case of Ar are more effective. It is expected, as the argon mass and ionization coefficient are higher than other gases studied.

Fig. 3 shows the dependence $j_i(U_d)$ of ion current density j_i on discharge voltage along the beam

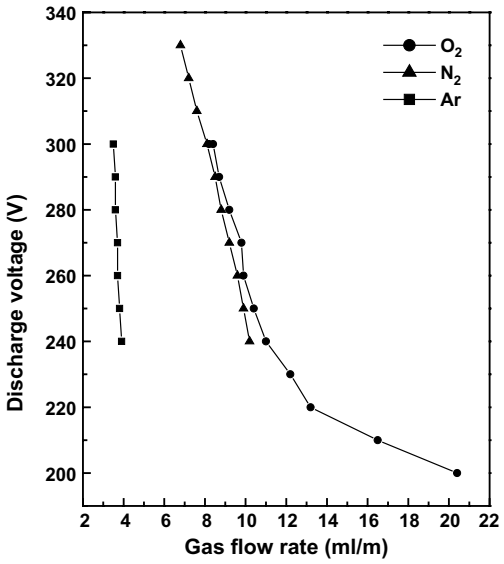

Fig. 2. Variation of discharge voltage with gas flow rate under constant discharge current for Ar, O_2 and N_2.

axis at the distance 15 cm from the source outlet with constant discharge current. The most interesting feature of the figure is the presence of maxima in the curves. The appearance of maxima becomes more evident, as the voltage should adjust with respect to the gas flow rate in order to keep the discharge current constant. But at sufficiently low voltages the ion current should tend to zero. The same is true for the opposite direction: increasing of the discharge voltage leads to decreasing of the gas flow rate (if there is no saturation) and at sufficiently high voltage (and, consequently, sufficiently low gas flow rate) the current should tend to zero again. So, it should achieve maximum somewhere in the intermediate point. In the Ar case the maximum is not well marked and this relates with the trend of the Ar discharge showing the saturation, which is seen from Fig. 2, where the curve for Ar is almost vertical. At the point of the upper end of the curve it seems the maximum appears but this mode is very unstable. However, in the case of Ar, higher the voltage higher will be the ion current, at least up to 290–300 V.

The angular distributions of the ICD along the plain at the distance 15 cm from the source outlet for investigated gases are presented in Fig. 4. The discharge voltages for Ar, O_2 and N_2 were 225, 270 and 260 V, respectively. For other voltages the distributions do not show any noticeable change and are quite similar. As we use different gas flow rates for different gases (because of the different voltages chosen) it will be useful to divide the ion current

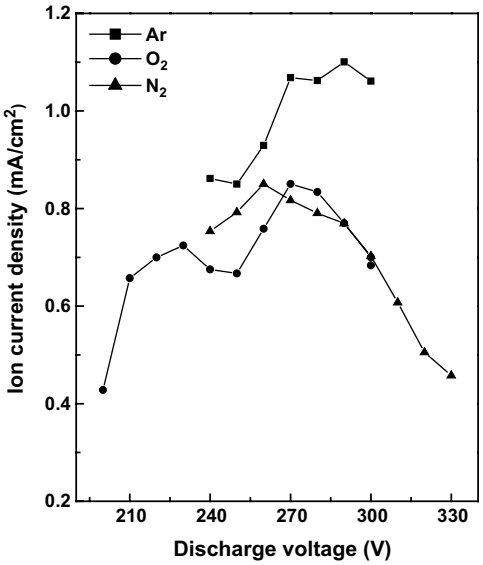

Fig. 3. Variation of ion current density with discharge voltage under constant discharge current for Ar, O_2 and N_2.

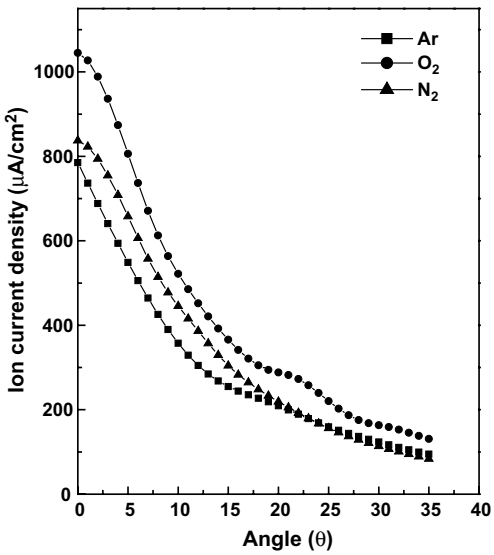

Fig. 4. Angular distributions of ion current densities for Ar, O_2 and N_2.

densities by corresponding gas flow rates for comparison. These reduced current densities are shown in Fig. 5.

Measured ICD for Ar in the studied SPT source is of the order of 1 mA/cm^2, which is two orders higher than that measured in conventional Kaufman-type ion source [9]. Other studied gases exhibit the close performances in SPT. To compare, we estimate the ionization lengths of the gases. For the electron temperature $T_e = 15$ eV, $\lambda_i = 3.3$ cm for Ar, 6.4 cm for O_2 and 6.6 cm for N_2 (the cross sections for Ar taken from [10] and for O_2 and N_2 from [11]. As the distance between the cathode and anode in our source is equal to 2.5 cm it is rather evident that the source should show good performance with Ar. The difference in λ_i between O_2 and N_2 shows, more complicated ionization processes taking place in the source with multi atomic molecules than only one parameter λ as it is described.

The results of ion energy analysis for Ar and N_2 are presented in Figs. 6 and 7, respectively. Distribution of ion beam energy was measured by using a retarding field analyzer. The average ion energy (E_{av}) and energy dispersion (σ) for Ar, calculated from Fig. 6, are $E_{av}^{Ar} = 160$ eV (70% of U_d) and

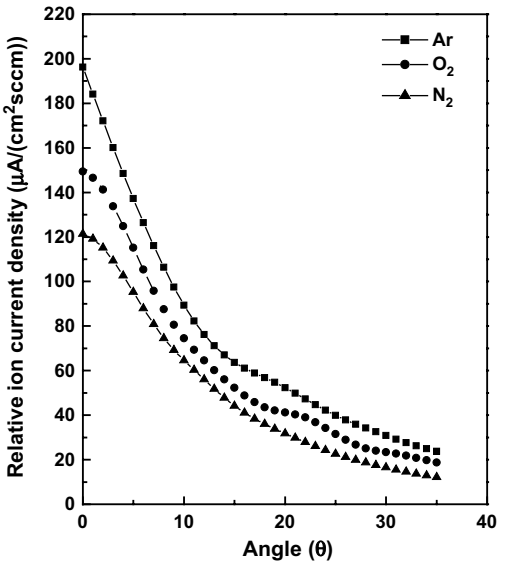

Fig. 5. Angular distributions of relative ion current densities for Ar, O_2 and N_2.

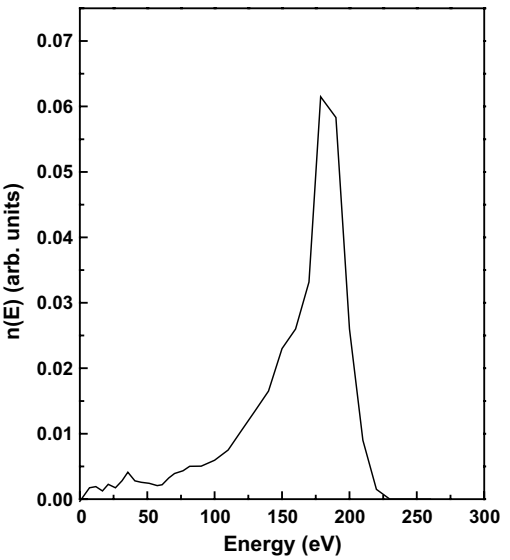

Fig. 6. Energy distribution of the Ar^+ ions in the SPT ion beam with the discharge voltage 230 V.

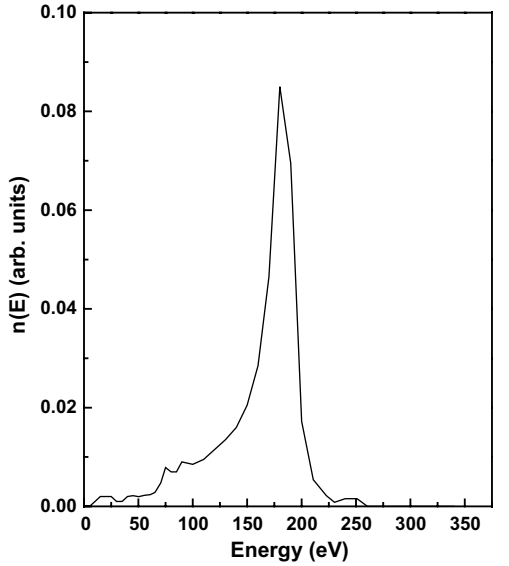

Fig. 7. Energy distribution of the N_2^+ ions in the SPT ion beam with the discharge voltage 260 V.

$\sigma_{Ar} = \pm 20$ eV, and those for N_2 calculated from Fig. 7 are $E_{av}^{N} = 160$ eV (60% of U_d) and $\sigma_{N_2} = \pm 18$ eV. The results with oxygen are analogous to these two gases.

4.2. Surface modification by SPT

4.2.1. PI surface

Fig. 8 presents the changes of the wetting angle when PI surfaces were irradiated with Ar^+, O_2^+ and N_2O^+ ions at different ion fluences. DI water and ethylene glycol drop of 9 μl were automatically dropped through 0.19 inner diameter nozzle of syringe and a wetting angle was measured by computer. Wetting angle was measured through computer by dropping about 9 μl of DI water and ethylene glycol on PI surface using syringe of 0.19 inner diameter nozzle. As shown in Fig. 8, the wetting angle of PI surface is reduced from 78° (non-treated PI) to 32° when inert Ar^+ ion beam is irradiated. When PI is irradiated with reactive O_2^+ ion beam with low current density of 0.5 mA/cm^2, the wetting angle quickly dropped to around 25° for the ion fluence of 5×10^{15}/cm^2 and remained at the same value for the fluence up to 1×10^{17}/cm^2 and it is then decreased to less than 10° for the fluence higher than 1×10^{17}/cm^2. The wetting angle is remarkably reduced to below 10° by reactive O_2^+ ion beam irradiation with the high current density of 0.8 mA/cm^2, even at the very low fluences. At fluences higher than 1×10^{17}/cm^2, the wetting angle becomes too small to be precisely measured. In case of N_2O^+ ion beam irradiation, the wetting angle drops to 28° for fluence 5×10^{15}/cm^2 and showed the same value for 1×10^{16}/cm^2. But at the ion fluence higher than 1×10^{16}/cm^2, the wetting angle abruptly decreases to 2°, which indicates that N_2O^+ ion is an effective ion species to reduce the wetting angle at relatively lower fluence than O_2^+ ion irradiation. Wetting angle is known to correlate with surface energy (γ), which is usually expressed as the sum of both polar force (γ_p) and dispersion force (γ_d). Using wetting angle parameters of DI water and ethylene glycol, surface energies of ion irradiated PI can be calculated by the adoption of the Owens–Wendt equation [12] and these results are presented in Fig. 9. As seen in Fig. 9, the surface energy of PI increases from 37 erg/cm to 69 erg/cm by Ar^+ ion irradiation. On the other hand, it is greatly raised up to 81.2 erg/cm by the irradiation of O_2^+ or N_2O^+ ion beam, which is two times higher than that of bare PI. This reveals that surface energy of the PI can be efficiently increased by reactive ion irradiation compared with an inert Ar^+ ion irradiation. This result agrees with previous reports that, keV ion irradiation on polymer surface in reactive gas environment increased the surface energy, in particular polar force by the increment of the amounts of hydrophilic groups (i.e. C═O) on modified surface [13,14].

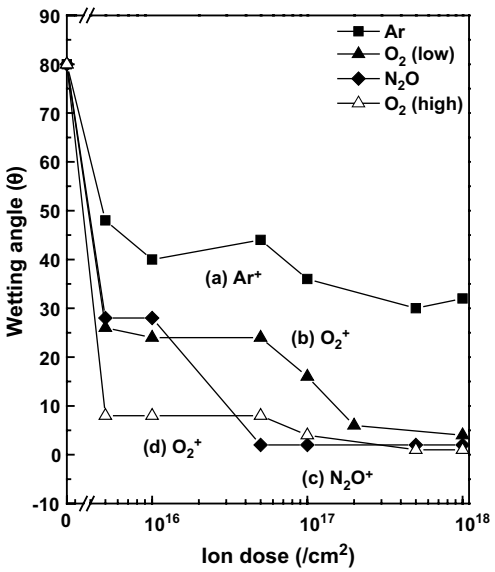

Fig. 8. Variations of wetting angles at various ion fluences for Ar^+, O_2^+ and N_2O^+ ion irradiated polyimide surface with 180 eV impinging energy (low and high correspond to the ion current density of 0.5 and 0.8 mA/cm^2, respectively).

In this study, O_2^+ ion beam energy of 180 eV is still so high enough to break the polymer chain on PI surface and in addition reactive atomic oxygen species resulting from dissociation after the collision with PI surface might participate in the formation of new chemical bonding with unstable broken chains. This assumption can be sufficiently supported by the increment of polar force in the O_2^+ irradiated PI surface compared to that of irradiated by Ar^+.

In case of N_2O^+ ion beam, two aspects of both chemical reaction and high mass transfer should be considered. Moreover, similar to O_2^+ ion beam impingement, N_2O^+ ion would be broken into several species like NO, O, N_2 and N at the collision on the PI surface. These reactive species actively

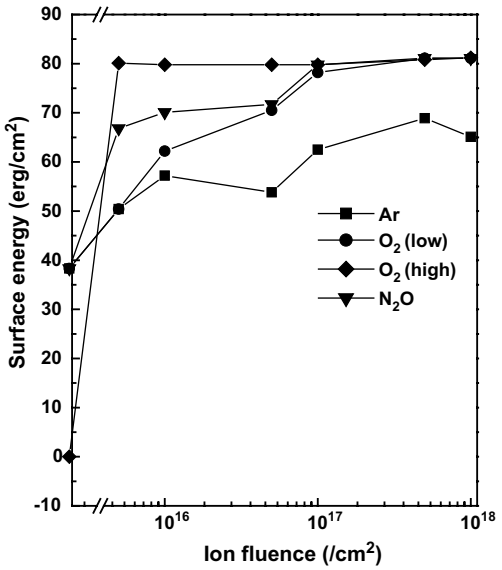

Fig. 9. Variations of surface energy at various ion fluences for Ar^+, O_2^+ and N_2O^+ ion irradiated polyimide surface with 180 eV impinging energy (low and high correspond to the ion current density of 0.5 and 0.8 mA/cm^2, respectively).

take part in forming the chemical bonding such as aromatic carbon bonded with O and N, carbonyl carbon and ether carbon etc and some of which improve the polar force of the PI surface. Such a dual effects of N_2O^+ ion beam irradiation make the wetting angle abruptly decreased to 2° at even low N_2O^+ ion fluence of 5×10^{16}/cm^2. At this fluence, Ar^+ and O_2^+ ion irradiation merely decrease the wetting angles as much as 44° and 25°, respectively. From the wetting angle measurement, low energy ion beam irradiation on PI shows much better performance for increasing the surface energy compared with previously reported surface treatment methods of plasma [15] and reactive ion etching [16].

Fig. 10 shows the evolution of C1s, N1s and O1s core-level spectra of bare and ion beam impinged PI surfaces by 1×10^{16}/cm^2 Ar^+, 5×10^{15}/cm^2 O_2^+ and 5×10^{16}/cm^2 N_2O^+ ions. C1s is comprised of four components, *heareafter* C_1, C_2, C_3 and C_4 features constrained to their values for clean PI. The component peak C_1, aromatic carbon, at 284.5 eV is attributed to the carbon atoms of two benzene rings of the ODA. The component peak C_2, aromatic carbon bonded N, at 285.3 eV is related to carbon atoms of the benzene ring in the PMDA and C—N bonding. Peak C_3 at 286.1 eV corresponds to a C—O single bond and peak C_4, carbonyl carbon, at 288.5 eV pertains to a C=O double bond. The oxygen O1s peak consists of two components, the carbonyl oxygen O_1 (C=O, 531.9 eV) and the ether oxygen O_2 (C—O—C, 533.2 eV). N1s is fitted into the imide group (400.1 eV) and iso-imide group (C—N—C, 398.8 eV). The energy difference 1.3 eV of fitted value coincides with the previous report on XPS spectra of PI irradiated by 0.1 keV oxygen ion beam [17]. Especially the ratio of carbonyl and ether oxygen by the fitting of O1s core-level spectra is estimated and the oxygen content in all the samples are increased from 14% for bare PI to higher than 29% after O_2^+ (high) ion irradiation and to about 28% for N_2O^+ ion irradiated PI surface at ion fluence 5×10^{16}/cm^2. From the results, the ratio of carbonyl O (C=O) increases from 9.9% of the bare PI surface to 18.3% and 17.08% for O_2^+ and N_2O^+ ion impinged PI surfaces, respectively. Direct irradiation of low energy reactive ion beam on PI was proved effectively to increase the atomic contents of hydrophilic C=O groups.

4.2.2. α-Al_2O_3(0001) surface

Fig. 11 shows XPS spectra of N1s core-level for the α-Al_2O_3(1000) treated by N_2^+ LIB with the ion beam energy 175 eV. The fluence is varied from 5×10^{15}/cm^2 to 1×10^{18}/cm^2. For N_2^+ irradiation on sapphire up to 5×10^{16}/cm^2, only one peak located at around 398.7 eV is observed and is related to non-bonded N_2 or NO bonding [18]. It is believed to result from N—N bonding of implanted N_2 not bonded with any Al or O, or NO molecule. After the irradiation of 1×10^{17}/cm^2, another peak is observed at the binding energy of 403 eV higher than N—N bonding and this results from the formation of Al—O—N. The intensity of Al—O—N shows steady increase with ion fluence up to 2×10^{17}/cm^2. After 5×10^{17}/cm^2, interestingly a new peak is observed at lower binding energy position than N—N bonding, which is located at 396.6 eV. Since the estimated binding energy difference between this peak and that of Al—O—N

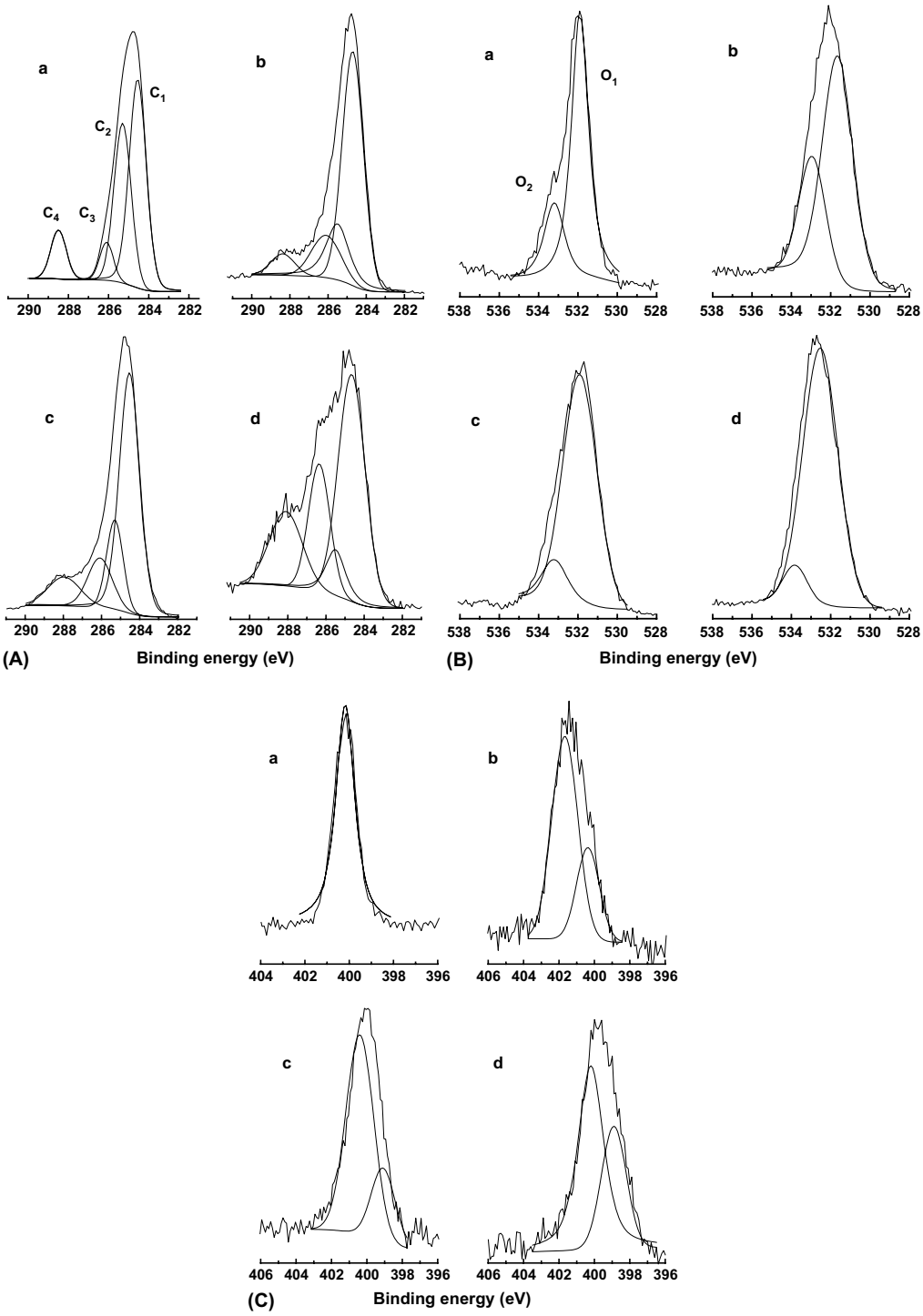

Fig. 10. Evolution of (a) C1s, (b) O1s and (c) N1s core-level spectra taken over the bare and ion beam impinged PI surfaces by $1 \times 10^{16}/cm^2$ (Ar^+), $5 \times 10^{15}/cm^2$ (O_2^+) and $5 \times 10^{16}/cm^2$ (N_2O^+). In each core-level spectra, (a)–(d) means bare, Ar^+, O_2^+(high) and N_2O^+ ion irradiated cases, respectively.

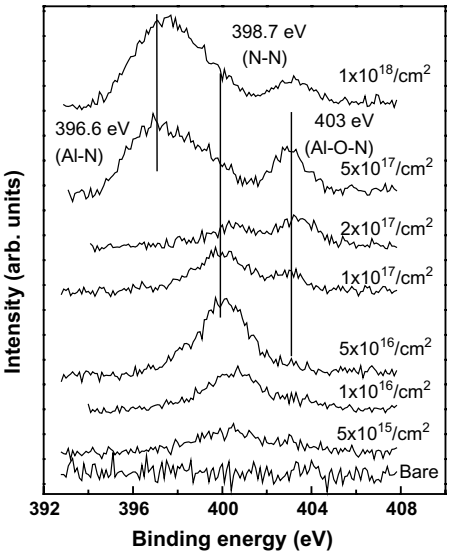

Fig. 11. N1s core-level X-ray photoelectron spectra of bare and N_2^+ ion beam treated sapphire substrates.

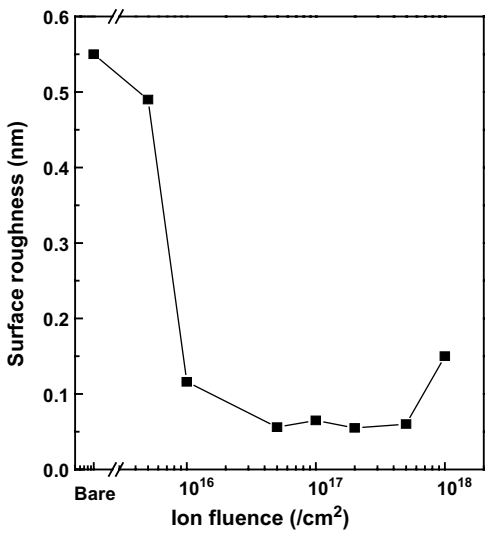

Fig. 12. Change of surface roughness of the bare and ion beam irradiated sapphire surfaces.

is about 6.4 eV, it can be obviously regarded as the Al—N bonding [19]. The peak intensity of Al—N is also increased after longer irradiation with fluence $1 \times 10^{18}/cm^2$ and the peak intensity ratio of Al—N to Al—O—N corresponds to 3.3. From the results it is clear that, low energy N_2^+ ion beam impingement on sapphire single crystal is very effective to form the functional layer on the surface and can produce different chemical bonding by the change of the ion fluence even at room temperature. In previous results [20], it is reported that only Al—O—N bonding was formed when low flux N_2^+ ion beam ($2\ \mu A/cm^2$) was irradiated on the sapphire single crystal using hollow cathode ion beam with ion beam energy higher than 500 eV and fluence over $5 \times 10^{16}/cm$. This also show that, even though ion beam energy is lower than 500 eV, high flux of ion beam current plays an effective role in the formation of Al—N bonding (enthalpy 297 kJ/mol). Fig. 12 represents the surface roughness variation with ion fluence for fluence from 5×10^{15} to $1 \times 10^{18}/cm^2$. The surface roughness was greatly diminished from 0.55 nm before the ion beam treatment to 0.11 nm just by the irradiation with low fluence $1 \times 10^{16}/cm^2$ and it seems to be saturated to as smooth as 0.1 nm up to $5 \times 10^{17}/cm^2$. But the surface became slightly rough again to 0.15 nm after long irradiation to $1 \times 10^{18}/cm^2$.

5. Conclusions

Investigations of the SPT-type plasma source show sufficiently high ion current density (two orders higher than in gridded sources [9]) with both noble (Ar) and reactive (O_2 and N_2) gases. The source has given rather broad ion beam with the average ion energy equal to 60–70% of the discharge voltage. The source is prospective for using in technological fields, where it is needed relatively soft and dense particle beams. As one of the applications, the surface energy of PI could be greatly increased from 37 erg/cm^2 to 81 erg/cm^2 by both O_2^+ and N_2O^+ beam irradiation generated by SPT, in which the processing time was also much reduced by 50–100 times than those of conventional ion sources of Kaufman and cold hollow type. Reduction of wetting angle is well explained by a large increase of carbonyl oxygen contents on ion irradiated PI surface. Moreover, Al—N and Al—O—N bonding could be successfully and effectively formed at room temperature through N_2^+ ion irradiation by SPT on α-$Al_2O_3(1\,0\,0\,0)$ single

crystal surfaces. As a summary, SPT with very low energy and high fluence can be regarded as a very useful ion source for surface modification of polymers and ceramics.

Acknowledgements

We acknowledge NIFS database for the data on nitrogen and oxygen ionization cross sections. The author, Won-Kook Choi appreciates the partial support from KIST, Flextronics Policy Program (2N27700) as well as the KOSEF under the contract (R01-2004-000-10715-0).

References

[1] H.R. Kaufman, R.S. Robinson, Operation of Broad-beam Sources, CSC, Alexandria, VA, 1987.
[2] A.I. Morozov, Physical Principles of Space Electro Jet Propulsion, Vol. 1, Atomizdat, Moscow, 1978 (in Russian); A.I. Bugrova, V.P. Kim, Plasma Accelerators and Ion Injectors, Nauka Publishers, Moscow, 1984, p. 107 (in Russian).
[3] A.I. Morozov, A.I. Bougrova, V.T. Niskine, A.V. Dessijatskov, D. Valentian, US5581155: Plasma accelerator with closed electron drift.
[4] L.A. Artsimovich et al., Kosmich. Issled. 12 (1974) 451 (in Russian).
[5] L.H. Caveny, F.M. Curran, J.R. Brophy, in: M. Perdu et al. (Eds.), Advanced Spacecraft Concepts Using Electrical Propulsion, 2nd German–Russian Electric Propulsion Conference, Moscow, Russia, 1993.
[6] A.I. Morozov, I.V. Melikov, J. Tech. Phys. 44 (1974) 544 (in Russian).
[7] A.I. Bougrova, Yu.A. Ermakov, P.V. Kolen'ko, in: Proceedings of the 3rd Russian–German Conference on Electric Propulsion Engines and their Technical Application, Stuttgart, Germany, 1994.
[8] V.S. Versotski, Yu.A. Ermakov, Physical processes in the plasma of the accelerator with closed electron drift during circuit oscillation, in: 2nd German–Russian on Electro Propulsion Engines and their Application, 16–21 July, Moscow, Russia.
[9] S.K. Koh, S.K. Song, W.K. Choi, H.-J. Jung, L. Gontcharov, Rev. Sci. Instr. 66 (1995) 5379.
[10] D. Rapp, P. Englander-Golden, J. Chem. Phys. 43 (1965) 1464.
[11] AMDIS database at NIFS databases. Available from: <http://dbshino.nifs.ac.jp>.
[12] D.K. Owens, R.C. Wendt, J. Appl. Polym. Sci. 13 (1969) 1741.
[13] W.K. Choi, S.K. Koh, H.J. Jung, J. Vac. Sci. Technol. A 14 (1996) 2366.
[14] S.K. Koh, S.C. Park, S.R. Kim, W.K. Choi, H.J. Jung, K.D. Pae, J. Appl. Polym. Sci. 64 (1997) 1913.
[15] A.M. Ektessabi, S. Hakamata, Thin Solid Films 377–378 (2000) 621.
[16] S. Iwamori, T. Miyashita, S. Fukuda, S. Nozaki, K. Sudoh, N. Fukuda, Vaccum 51 (1998) 615.
[17] R. Flitsch, D.-Y. Shin, J. Vac. Sci. Technol. A 8 (1990) 2376.
[18] D. Briggs, M.P. Seah, Practical Surface Analysis, John Wiley, New York, 1984.
[19] A.D. Katani, K.I. Papathomas, J. Vac. Sci. Technol. A 5 (1987) 1335.
[20] W.K. Choi, H.-J. Jung, S.K. Koh, D. Byun, D.-W. Kum, J. Vac. Sci. Technol. A 16 (1998) 3311;
W.K. Choi, S.K. Koh, H.-J. Jung, J. Vac. Sci. Technol. A 17 (1999) 3363.